

Fusing Echocardiography Images and Medical Records for Continuous Patient Stratification

Nathan Painchaud, Jérémie Stym-Popper, Pierre-Yves Courand, Nicolas Thome, Pierre-Marc Jodoin, Nicolas Duchateau, and Olivier Bernard

Abstract—Deep learning enables automatic and robust extraction of cardiac function descriptors from echocardiographic sequences, such as ejection fraction or strain. These descriptors provide fine-grained information that physicians consider, in conjunction with more global variables from the clinical record, to assess patients' condition. Drawing on novel transformer models applied to tabular data, we propose a method that considers all descriptors extracted from medical records and echocardiograms to learn the representation of a cardiovascular pathology with a difficult-to-characterize continuum, namely hypertension. Our method first projects each variable into its own representation space using modality-specific approaches. These standardized representations of multimodal data are then fed to a transformer encoder, which learns to merge them into a comprehensive representation of the patient through the task of predicting a clinical rating. This stratification task is formulated as an ordinal classification to enforce a pathological continuum in the representation space. We observe the major trends along this continuum on a cohort of 239 hypertensive patients, providing unprecedented details in the description of hypertension's impact on various cardiac function descriptors. Our analysis shows that i) the XTab foundation model's architecture allows to reach outstanding performance (98% AUROC) even with limited data (less than 200 training samples), ii) stratification across the population is reproducible between trainings (within 3.6% MAE), and iii) patterns emerge in descriptors, some of which align with established physiological knowledge about hypertension, while others could pave the way for a more comprehensive understanding of this pathology.

Index Terms—Multimodal, transformer, stratification,

representation learning, cardiac ultrasound, health records, hypertension

I. INTRODUCTION

WHEN assessing patients' condition, physicians draw upon their expertise to integrate relevant complementary data from various sources such as medical images and Electronic Health Records (EHRs) [1] into a global picture of the patient's status. Such a clinical workflow is typical in cardiology for the characterization of hypertension (HT), a complex and multifaceted disease. While HT is the most prevalent cardiovascular disease (CVD), affecting around 1.28 billion adults worldwide [2], it presents a complex pathophysiology involving multiple mechanisms and is associated with other risk factors of CVDs. Although the diagnosis for HT is based on widely recognized thresholds of measured blood pressure (BP), the concrete risk of cardiovascular events related to HT is less clearly understood. Different rule-based scores have been proposed to estimate these risks, but they are based on limited numbers of risk factors, on top of requiring calibration to adjust to different populations [2]. For these reasons, there is clinical interest in developing models that can integrate multiple parameters of cardiac health to characterize precisely the HT continuum.

So far, most deep learning methods for cardiac applications have focused on a limited number of modalities to solve highly-specific tasks, such as the automatic extraction of shape and motion/deformation parameters from MR and ultrasound images [3]–[5]. Some methods combine the detail-rich imaging data with other sources, but they often sacrifice lots of information, for example by using single frames from whole 3D volumes or 2D+time sequences [6], [7] or by resuming images to a few scalar biomarkers [1], [8]. Furthermore, the most successful multimodal approaches leverage large datasets, while models trained on small datasets targeting specific pathologies, as is our case with HT, often lead to poor fitting [9]. Thus, the sheer difficulty of efficiently combining highly heterogeneous and limited data means that research on comprehensive models to aid higher-level diagnosis has lagged behind [10].

A category of deep learning models that has shown promising results in multimodal applications is transformers. Since the transformer architecture makes no assumptions about the structure of the data, different data sources can be combined naturally inside one framework [11]. Even if their are

Manuscript received October 11, 2024; revised XXXX XX, 2024. This work was supported in part by the NSERC's Discovery Grants and Canada Graduate Scholarships-Doctoral programs, the FRQNT Doctoral Training Scholarships and the French National Research Agency (LABEX PRIMES [ANR-11-LABX-0063] of Université de Lyon, within the program "Investissements d'Avenir" [ANR-11-IDEX-0007], and the MIC-MAC [ANR-19-CE45-0005] and ORCHID [ANR-22-CE45-0029-01] projects). For the purpose of open access, the authors have applied a CC BY public copyright license to any Author Accepted Manuscript (AAM) version arising from this submission.

N. Painchaud, P.-Y. Courand, N. Duchateau, and O. Bernard are with Univ Lyon, INSA-Lyon, Université Claude Bernard Lyon 1, UJM-Saint Etienne, CNRS, Inserm, CREATIS UMR 5220, U1294, F-69621, Lyon, France (e-mail: nathan.painchaud@usherbrooke.ca).

N. Painchaud and P.-M. Jodoin are with the Department of Computer Science, University of Sherbrooke, Sherbrooke, QC, Canada.

J. Stym-Popper and N. Thome are with Sorbonne Université, CNRS, ISIR, F-75005, Paris, France.

P.-Y. Courand is also with the Cardiology Dept., Hôpital Croix-Rousse, Hospices Civils de Lyon, Lyon, France, and the Cardiology Dept., Hôpital Lyon Sud, Hospices Civils de Lyon, Lyon, France.

N. Thome and N. Duchateau are also with the Institut Universitaire de France (IUF).

innately suitable for multimodal applications, they remain competitive with their domain-specific counterparts [11], [12]. Transformers even broke through in domains where deep learning based approaches previously struggled against simpler machine learning solutions, such as tabular data [13].

However, in practice, the lack of assumptions about the data means that transformers are trained on larger datasets, allowing them to learn the interactions within the data without any enforced prior [11], [14]. While this adaptability is at the heart of their success, it exacerbates the issue of the availability of [labeled] data on which to train the models, especially in healthcare. A recent development that could unlock the potential of transformers for medical applications came with *foundation models*. These are models pretrained on enormous quantities of varied data to learn generic patterns, under the assumption that they can efficiently adapt to downstream tasks with limited quantities of domain-specific data [15].

In this paper, we propose to leverage transformers to combine a small dataset of EHR data and detailed cardiac function descriptors extracted from 2D+time echocardiographic sequences to continuously stratify HT. We built our method around the representation of EHR data in a tabular format, adding a dedicated branch to integrate image-based data to this representation. We also use the ordering of the labels in the supervised objective to predict a position along a pathological continuum, learning a more instructive representation of patients in the process. Finally, we showcase how this continuous representation can help discover new subtle indicators of hypertension's progress.

Our main contributions in this work are:

- 1) A framework to fuse tabular data extracted from EHRs with tabular and time-series parameters extracted from 2D+time Apical 4 Chambers (A4C) and A2C echocardiographic sequences¹, justified by ablation studies of each component;
- 2) A study of multimodal strategies in a limited data setting, showcasing: i) the usefulness of first extracting relevant descriptors from images, and ii) the stark improvement (over 10 points in AUROC) of our method over current state-of-the-art;
- 3) Using an ordinal classification constraint on high-level ordered labels to represent the pathological continuum;
- 4) A promising case study of this continuous stratification on hypertension, showing emerging patterns, both known and new, that mark the progression of hypertension.

II. RELATED WORK

A. Multimodal Machine Learning

Multimodal learning encompasses multiple techniques for combining heterogeneous data for downstream tasks. Our HT application aims to *fuse* complementary EHR and imaging data to learn a *joint* representation from which to make predictions [16]. In other cases, it might be preferable to learn separate *coordinated* representations for each modality and *align* them using similarity measures [6], [16].

Most current papers on multimodal learning apply to combinations of [non-medical] visual, text and audio data [16], since these modalities are cheap to acquire and abundant online. In the medical domain, Zhou *et al.* recently introduced IRENE [17], a multimodal transformer for disease diagnosis with a custom cross-attention component between images and unstructured textual EHR data. Because of its size, IRENE was trained on a large dataset of over 44K subjects. However, medical applications often have less samples available, though with more structure to leverage in EHR data than raw text. Thus, Hager *et al.* [6] and Schilcher *et al.* [7] both introduced multimodal frameworks designed for medical tabular and imaging data, rather than adapting generic multimodal models designed for vast quantities of natural images and text. The method proposed by Hager *et al.* presents components similar to ours, such as contrastive learning inspired by SCARF [18], but they aim to align modalities rather than fuse them. As for Schilcher *et al.*, they implemented multiple fusion schemes (i.e. early, mid and late) to show slight, but systematic, improvements over unimodal image predictions. In both cases, they still used large medical databases, with over 40K subjects in the case of Hager *et al.*, and 1 073 for Schilcher *et al.*. Therefore, even methods developed for healthcare data are likely to run into significant issues when applied to our problem. Despite our specific use-case, we can draw relevant inspiration from conclusions that have emerged from the medical and general multimodal fusion literature.

For multimodal fusion applications, *mid-fusion* approaches have shown promising results [17], [19]. They consist in having intermediate neural network layers independently extract features from each modality, before the features are joined and processed by further layers. By contrast, in *early fusion* the feature extractor components are frozen, and cannot learn features adapted to the fusion task [20]. Despite the adaptability of mid-fusion, the biomedical community still favors early fusion [9], [20], since it can be achieved by simply joining features extracted using pretrained models [20].

Another takeaway from the literature is the intrinsic advantages of transformers for multimodal applications [11]. Indeed, the lack of assumptions regarding the structure of the data allows them to scale well to different modalities, compared to the spatial structure bias of convolutional networks. In light of the advantages listed above, our data fusion pipeline described in section III is built around the transformer framework.

B. Patient Stratification

The task of predicting the outcome or pathological stage of patients is known as *stratification* [21]. Often, stratification models use large quantities of unstructured EHR data or medical images to unveil emerging patterns, as recently demonstrated on the EHRs of more than 1.6 million patients [22]. However, studies have highlighted that models with such broad scopes risk under-performing on rare subtypes [23]. This shortcoming of broad models justifies the existence of methods with more targeted applications, for which available data is typically labeled but much more rare.

In cardiology specifically, deep learning models have mostly focused on quantifying imaging data, rather than stratifying

¹Code is available at *URL to be disclosed upon publication*

patient risk based on reference labels [21], [24]. Recently, some works tackled unsupervised phenotyping using representation learning and clustering, in particular for hypertension characterization [22], [25]. The different properties of supervised and unsupervised stratification methods lead to a dilemma. Unsupervised methods are able to learn rich and continuous representations, which can highlight gradual alterations in biomarkers [25]. Nevertheless, their representations might not align with established clinical labels known by clinicians. Supervised approaches are anchored to such clinical labels [21]. Unfortunately, they can lead to low-density regions outside of the clustered labels, missing patterns in transitions between clusters. However, supervised methods typically ignore the ordering of stratification labels, e.g. from best to worst outcome, which could help structure their representation.

This neglected information explains why some works formulate stratification as an ordinal classification problem, where the ordering of the labels is taken into account. The downside is that, until recently, such methods implied more complex models and/or optimizations, and practical implementations were limited to linear models [26]. Recently, ordinal classification was adapted to deep learning in a simple formulation applicable on top of any feature-extractor architecture [27].

III. METHOD

Figure 1 summarizes our pipeline. The echocardiograms are first segmented (1a) and numerical and time-series descriptors are extracted (1b). For health records data, we manually extracted categorical (e.g. sex, medical history, etc.) and numerical descriptors (e.g. age, BMI, etc.) from EHRs and a posterior assessment by a cardiologist (1c).

Our approach for modeling multimodal interactions is somewhat similar to the *hierarchical attention (multi-to-one stream)* described in [11]. Each modality is processed independently (figs. 2a and 2b) before being fed to an encoder (fig. 3) that performs data fusion and outputs a joint embedding for downstream tasks.

Since we are interested in learning a meaningful latent representation at the output of the encoder, we use a specific formulation of the supervised training objective in our pipeline. Indeed, we frame the prediction of the stratification labels as an ordinal classification to integrate the stratification notion in the latent representation. With this, we obtain a continuous value between 0 (healthy) and 1 (severe disease) for each patient, indicating the model’s prediction along the pathological continuum. This formulation allows for an efficient traversal of the manifold without having to resort to ad hoc methods.

Below, we describe steps 3 through 5 illustrated in fig. 1. Since steps 1-2 and 6 are application-specific, as they relate to the dataset and post hoc evaluation, they are further explained in sections IV-A, IV-B and V-B, respectively.

A. Multimodal Tokenization (Step 2)

From the application’s perspective, our framework operates on images and EHR data. As mentioned above, these raw data are pre-processed to extract i) time-series descriptors from

images (series of scalar values per patient), and ii) tabular descriptors from EHRs and images (global categorical and numerical variables per patient). Given the fundamentally different structures of these data types, we split the tokenization in two streams (S_{time} and S_{tab}), one for each modality (cf. fig. 2).

1) Time-Series Tokenizer: Under the assumption that there are (possibly complex) patterns in time-series descriptors during the cardiac cycle, they require modality-specific processing to be properly extracted. Therefore, we took inspiration from how Pellegrini *et al.* integrated longitudinal data in their multimodal transformer [1] for the design of our time-series tokenizer module, detailed in fig. 2a.

Starting with a vectorized input sequence $\mathbf{t} \in R^T$, each scalar in \mathbf{t} is upsampled to the embedding size D through a linear layer. This D -fold increase in dimensionality is not meant to transform the data, but rather to structure it so that downstream attention operations can more meaningfully process it. Thus, the sequence, now made up of T tokens of size D , is combined to a positional encoding before being fed to a transformer block. Finally, the T output tokens are reduced to a single D -dimensional token — the embedding for the time-series — using sequence pooling, i.e. a dynamic weighted averaging [29]. Since all the time-series descriptors represent the same type of data, i.e. cyclical 1D signals, the weights of their tokenizer are shared between time-steps and descriptors.

2) Tabular Tokenizer: The recent FT-Transformer framework by Gorishniy *et al.* [13] achieved state-of-the-art results on various tasks involving tabular data. Therefore, we adopted their Feature Tokenizer for tabular data, illustrated in fig. 2b.

Tabular data is represented so that each descriptor/column maps to a token. This means that each patient/row corresponds to a sequence of tokens that can be processed by a transformer. Thus, tokenization upsamples each descriptor to a D -dimensional token. For categorical descriptors, the upsampling operation is an embedding layer, i.e. a dictionary of embedding vectors for each label to add to a shared bias. For numerical descriptors, it is a linear layer. To learn distinct embeddings for each descriptor, the parameters are not shared between descriptors.

B. Transformer Encoder (Step 3)

The tokenization described in section III-A outputs two sequences of tokens (one per modality). Our pipeline concatenates both sequences and a [CLS] token to get one sequence of $S + 1$ tokens, where $S = S_{\text{time}} + S_{\text{tab}}$, which is fed to a transformer encoder, detailed in fig. 3.

The combination of the transformer backbone and data representation grants flexibility to the model. Since input descriptors map to tokens, and transformers adapt to token sequences of various lengths, the same backbone can be re-used across different configurations of input data.

1) Multimodal Token Fusion: Our recommended pipeline simply concatenates tokens from different modalities before the self-attention transformer encoder. As an alternative, we tested a state-of-the-art multimodal transformer module. It

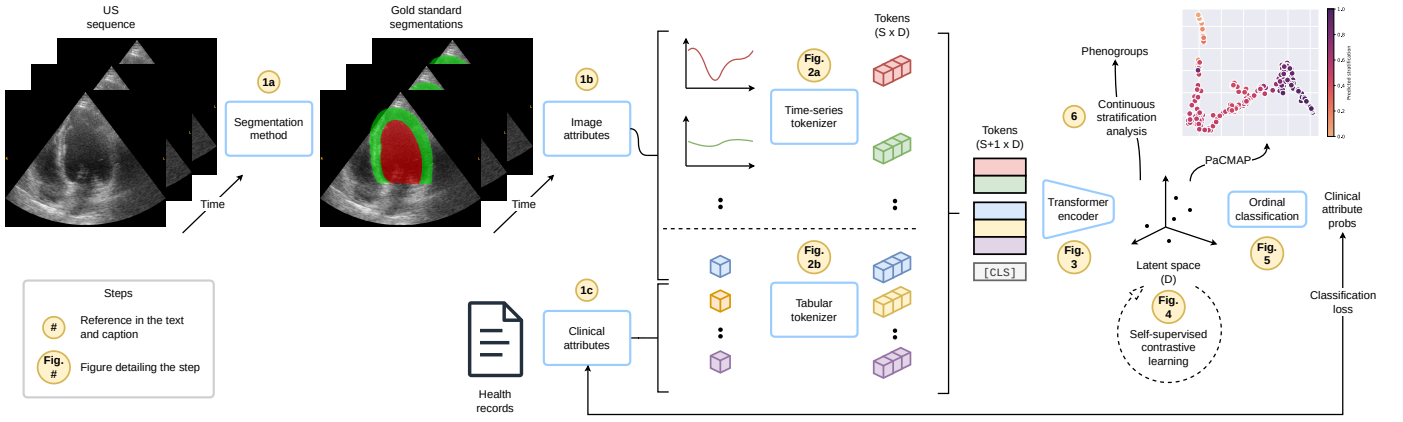


Fig. 1: Schematic representation of our multimodal fusion pipeline. The echocardiograms are segmented (1a) and descriptors are extracted from them (1b). In parallel, health records data are structured into categorical and scalar descriptors (1c). Time-series descriptors (w.r.t. the cardiac cycle) and tabular descriptors are processed into individual embeddings using modality-specific methods (fig. 2a, fig. 2b). The embeddings are then fed to a transformer encoder (fig. 3) trained to predict a probability distribution that takes into account the ordering of the target classes (fig. 5). The learned representation can finally be analyzed w.r.t. the predicted stratification (6) or visualized using dimensionality reduction (PaCMAP [28]).

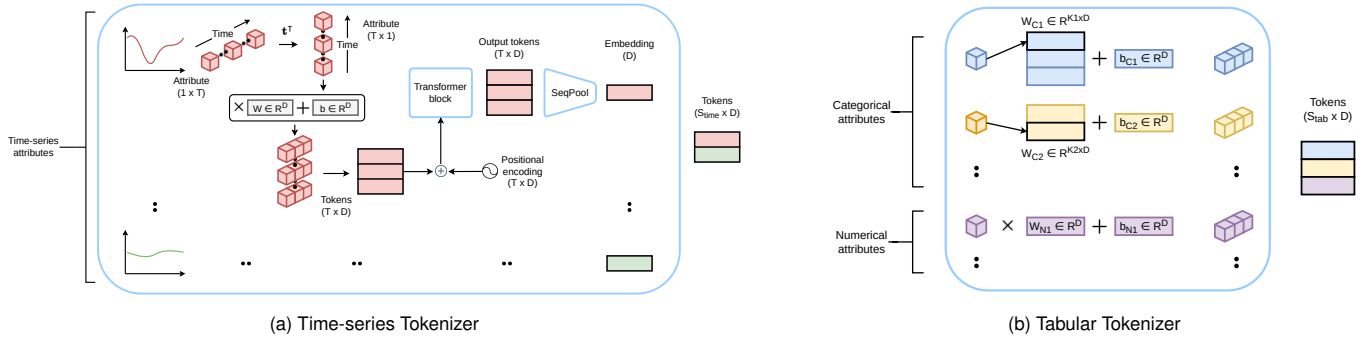


Fig. 2: Details of the two modality-specific tokenization methods for embedding multimodal data. The output of each method is a sequence of tokens of length equal to the number of input descriptors for each modality: S_{time} and S_{tab} for time-series and tabular descriptors, respectively.

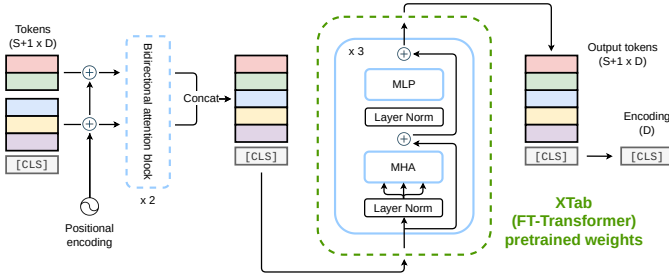


Fig. 3: Architecture of the transformer encoder pipeline from figs. 1 and 4. The tokens, initially separated by modality, can optionally pass through bidirectional multimodal attention blocks proposed in [17], before being concatenated into one unified sequence of tokens. They are then fed to self-attention transformer blocks. In experiments using the configuration from the XTab foundation model [14], these blocks (inside green dashes in the figure) can optionally be initialized by the pretrained weights from XTab. In all configurations, other components, such as the [CLS] token, positional encoding, and tokenizers, and more, are initialized randomly.

consists of bidirectional multimodal attention blocks, a cross-attention module introduced in the IRENE model [17], which performs symmetric cross-attention on both modalities before concatenating tokens. This optional component can be added as shown in fig. 3, and its impact is discussed in section V-A.3.

2) FT-Transformer & XTab Foundation Model: Once tokens are combined into one “unimodal” sequence, we use a

vanilla transformer encoder, like in the FT-Transformer framework [13]. The configuration — number of layers, token size, normalization, etc. — was chosen to follow the one used by XTab, a foundation model built on a FT-Transformer backbone [14].

XTab’s approach to generalization differs from that of other foundation models in domains such as natural language processing (NLP) and CV [14]. Since the meaning and context of tabular data varies between datasets, XTab foregoes learning a universal tokenizer, focusing instead on learning a weight initialization that generalizes well to downstream tasks. The pretrained weights provided by XTab only include the transformer blocks, indicated by the green box in fig. 3, since they do not depend on the types and number of input features. Other parameters specific to the task or data, such as tokenizers or the [CLS] token, are learned from scratch.

To initialize its weights, XTab is trained, in a self-supervised manner, to reconstruct features from 52 tables from the AutoML benchmark (AMLB) [30]. Between tables, the size of the data varies greatly in terms of numbers of rows (between 10 and 10,000,000) and columns (between 4 and 14,892).

3) Self-Supervised Contrastive Pretraining (Step 4): As an alternative to pretrained weights trained on external data, our framework can use self-supervised contrastive learning to pretrain on our own dataset (cf. fig. 1 (4b)). Our contrastive

pipeline, detailed in fig. 4, corresponds to a mix of the methods proposed by SCARF [18] and MTR [31].

C. Ordinal Classification (Step 5)

One goal of our method is to provide a continuous stratification of HT severity. To achieve this, we use the implicit information in the ordering of discrete labels provided by an expert cardiologist. Our method is constrained to learn a continuous representation along which patients are ordered w.r.t. HT severity labels by relying on the ordinal classification formulation proposed by Beckham and Pal [27], detailed in fig. 5. Given the features extracted by the encoder, a linear prediction head predicts the parameter $p \in [0, 1]$ of a binomial distribution, instead of logits. The logits are computed analytically given p using the binomial probability mass function. This allows the constrained prediction head to be used with standard classification losses, like cross-entropy.

This formulation means p directly determines the label with the most probability mass, and reducing/increasing p shifts the probability mass center towards earlier/later labels in the ordering, respectively. Therefore, p can be used as continuous stratification, rather than convert it to probabilities over the labels. Figure 6 contrasts an embedding of the patients colored w.r.t. discrete labels (a) and p (b), illustrating how our method manages to learn a continuous representation structured around the labels. Since the prediction head is linear, it forces a direction along the latent representation to correspond to the order of target labels, clearly visible in fig. 6a.

IV. EXPERIMENTAL SETUP

A. Dataset

To evaluate our pipeline, we used an in-house dataset of echocardiographic sequences and EHR data collected from 239 hypertensive patients (CARDINAL cohort). The studies involving human participants were reviewed and approved by the local ethics committee. The participants provided their written informed consent to participate in this study. The CARDINAL imaging data was first introduced by Ling *et al.* to train a 2D+time nnU-Net using pseudo-labels [5].

For the current study, we included an additional 62 numerical and categorical descriptors, extracted from an EHR server or derived from other descriptors. The descriptors cover various aspects of the patients' condition, from general information (e.g. age, sex, etc.), medical history (e.g. stroke, tobacco, etc.), and biological reports (e.g. NT-proBNP, etc.) to measures from hospital stays (e.g. 24-hour ambulatory blood pressure) and transthoracic echocardiograms (e.g. A4C, PLAX, etc.). All the descriptors are described in tables V to VII in the supplementary materials.

We used the HT severity descriptor as prediction target. It represents three degrees of hypertension assessed post hoc by an expert cardiologist. The labels, in ascending order of severity, are: i) *wht* (White coat HyperTension), no positive diagnosis of hypertension, ii) *controlled*, patients whose hypertension is under the recommended blood pressure level given their treatment, and iii) *uncontrolled*, patients who remain above the recommended blood pressure level despite treatment.

B. Echocardiograms Processing

As described in section III, the 2D+time echocardiographic sequences are first segmented, from which global and frame-by-frame cardiac function descriptors are automatically computed. For the segmentations, we use the state-of-the-art masks predicted by the nnU-Net from Ling *et al.* [5] as gold-standard. The descriptors were chosen by a cardiologist based on their relevance for assessing HT. The scalar descriptors measured on the patients are the following:

- (2 *descriptors*) Left Ventricle (LV) volumes at End-Diastole (ED) and End-Systole (ES), using Simpson's biplane method [33];
- (1) Ejection Fraction (EF) from LV ED/ES;
- (8) Minimum/maximum myocardial curvature of the walls (A4C: septal/lateral, A2C: inferior/anterior) at ED [34], in both A4C and A2C views.

The time-series descriptors measured on both A4C and A2C views are:

- (2 \times 1 *descriptor*) Surface of the LV;
- (2 \times 1) LV length along its main axis (base to apex);
- (2 \times 3) Global strain and regional strain, with the local segments depending on the view (A4C: septal/lateral, A2C: inferior/anterior);
- (2 \times 2) Local average myocardial thickness, with local segments depending on the view (A4C: septal/lateral, A2C: inferior/anterior).

We define the septal/lateral and inferior/anterior segments as the first 30% of the myocardium from base to apex on each side, just as in [34]. Because we are not doing tracking, we split the myocardium into longitudinal segments by sampling equidistant control points along the myocardium and selecting a subset of control points.

C. Framework Configuration

1) *Transformer Encoder*: We tested two main configurations for the architecture of the transformer encoder. Given the best configuration, we also performed ablation studies of our pipeline's components. The configurations are described here, and their performance are discussed at length in section V-A.

One of the transformer encoder architecture we tested was the exact FT-Transformer configuration proposed by XTab [14]. The important parameters are an embedding size of 192, 3 transformer blocks, and 8 heads in Multihead Self-Attention (MSA) layers. We use the training/finetuning hyperparameters recommended in [14], with a 2000 steps limit and a cross entropy classification loss function.

Given the large size of XTab (~1.1M parameters) compared to our training samples (<200), we also tested a much smaller FT-Transformer configuration (~5K parameters). We performed a hyperparameter search over the configuration options for a "tiny" model, and found an embedding size of 8 (vs 192), 6 transformer blocks (vs 3), and 2 attention heads (vs 8) to be optimal. This model is trained with the same hyperparameters, but with a LR finder and 2500 steps. When pretraining, contrastive pretraining lasts 2500 steps, followed by finetuning with supervised labels for 500 steps.

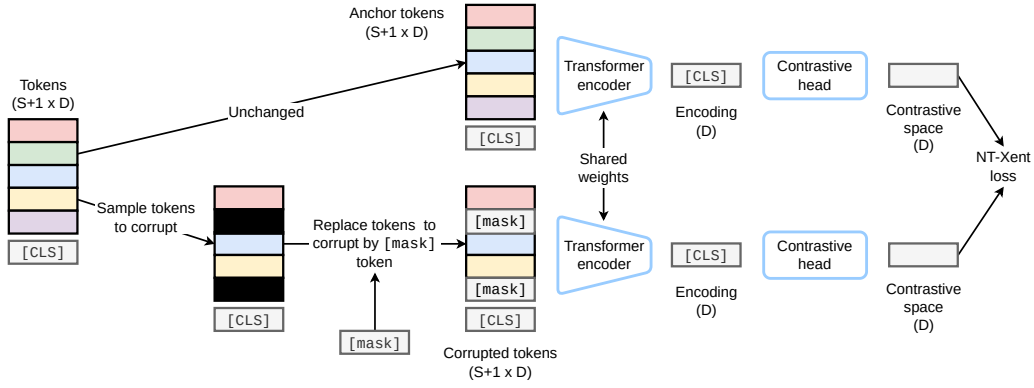


Fig. 4: Schematic representation of the self-supervised contrastive pretraining framework from fig. 1. It is inspired by SCARF’s contrastive learning for tabular data [18]. Instead of augmenting both views like SimCLR [32], one *anchor* view corresponds to *unchanged* tokens, and a *corrupted* view is generated by perturbing randomly sampled tokens. Rather than corrupting tokens by replacing them with samples from the corresponding input data’s marginal distribution, we replace them by a universal learnable `[mask]` token, as proposed in [31].

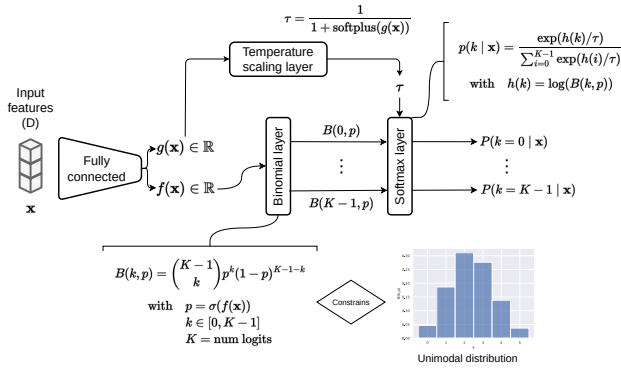


Fig. 5: Details of the ordinal classification from fig. 1 (5). Given a feature vector \mathbf{x} , the goal is to output probabilities over the classes $p(k | \mathbf{x})$ following a unimodal distribution, meaning the probabilities should gradually decrease on both sides of the class predicted as most likely. Instead of logits, the model predicts the parameter $p \in [0, 1]$ of a binomial distribution. The binomial probability mass function $B(k, p)$ is used to compute the probabilities for the K classes, ensuring a unimodal distribution. Finally, a softmax is applied on the probabilities to sharpen/flatten their distribution, based on a temperature τ also predicted by the model. In the end, the probabilities $p(k | \mathbf{x})$ can be used with standard classification losses.

2) Other Components: Aside from the transformer encoder itself, we tested other configurations aspects, listed below. These components’ impact is discussed later in section V-A.

- **Input data:** Given our wealth of tabular data, we studied the impact of the presence or absence of certain descriptors. We defined subsets of tabular descriptors to provide to models. All 62 tabular descriptors are referred to as *all*. Many of these descriptors come from ultrasound exams, e.g. measures of cardiac structures performed by experts on echocardiograms. Leaving out these descriptors, we obtained 28 descriptors *w/o echo. data*;
- **Image descriptors tokenization & fusion:** We stated in section III-A.1 that time-series descriptors require modality-specific processing. To validate this, we compared our time-series transformer tokenizer to an approach that linearly projects time-series to the tokens’ D -dimensional embedding. Concurrently, we tested adding

bidirectional multimodal attention blocks, given their reported success on medical data [17], to see if first mixing modalities’ information through cross-attention could offset the lack of modality-specific processing;

- **Latent representation:** We investigated the optimal way to extract a representation from transformer features, between using `[CLS]` token and performing a weighted average of all output tokens using sequence pooling. At the same time, we tested the impact of the *ordinal constraint*, described in section III-C, compared to the classification head proposed by the FT-Transformer [13] with a cross-entropy loss.

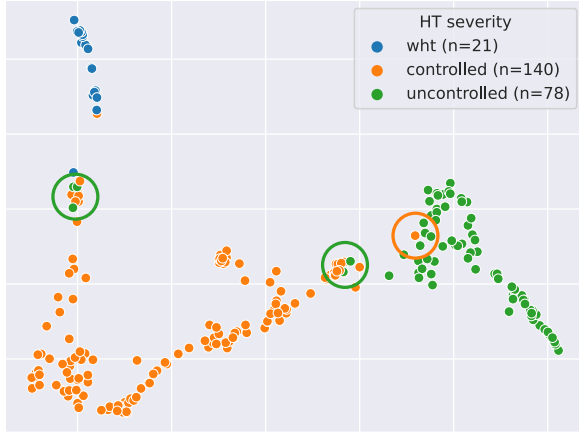
D. State-of-the-art Comparisons

Aside from ablation studies of our proposed framework, we compare it to two relevant state-of-the-art methods, first mentioned in section II-A. Both of these methods are summarized below, as well as how they were adapted to work with our data. The results of all three methods are discussed in section V-A.

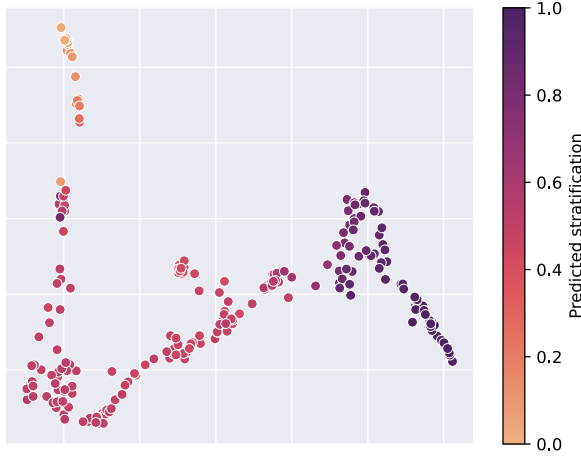
1) Image-centered Framework: To assess the benefit of extracting clinically relevant time-series descriptors from images, we tested the multimodal pipeline proposed by Hager *et al.* [6], meant to work with images directly. They encode images and tabular data separately using a ResNet50 and MLP, respectively, before aligning both sets of features using a contrastive strategy. Classification is performed by a linear layer on top of the image features. At test-time, only the image branch and linear classifier are used.

This method is meant for 2D images, with the authors selecting important slices when dealing with 3D images. To be fair in our comparison and provide temporal information, we concatenate the 4 most important frames of each patient (i.e. End-Diastole (ED) and End-Systole (ES) frames from both A4C and A2C views) as different channels to the ResNet50.

2) Multimodal Transformer: We also tested IRENE [17], a state-of-the-art multimodal transformer model for healthcare data. IRENE was originally tested on images and a combination of structured and unstructured clinical data. They first process tokens with blocks mixing cross-attention and self-attention modules, called *bidirectional multimodal attention*,



(a) Embedding colored w.r.t. the target degrees of hypertension, ordered in the legend by their severity (cf. section IV-A). Some patients appearing outside of their respective regions in the latent space are misclassified. They are circled in the colors of their reference labels to highlight them.



(b) Embedding colored w.r.t. the continuous stratification predicted by our method, where 0 (light) corresponds to healthy subjects, and 1 (dark) corresponds to the most hypertensive patients.

Fig. 6: 2D visualization, using the PaCMAP dimensionality reduction algorithm [28], of the 192D latent space learned by our transformer encoder, each point corresponding to a patient.

before standard self-attention blocks on the concatenated tokens from both modalities.

Even though IRENE was tested on data of a different nature than our application, its transformer backbone allowed us to swap in our time-series and tabular data tokens, to compare only their multimodal fusion encoder to ours.

V. RESULTS

A. Multimodal Fusion Framework

Tables I to IV present the results of ablation studies on our proposed pipeline, described in section IV-C, and comparisons with state-of-the-art multimodal methods for imaging and clinical data, described in section IV-D. The results correspond to the area under the receiver operating characteristic curve (AUROC) for the HT severity labels (cf. section IV-A) on a hold-out test set of 48 patients, corresponding to around 20% of the dataset. In the following subsections, we analyze the

changes in performance given the different configurations of each component, starting with the most impactful ones. At the same time, we also discuss the properties of our framework highlighted by these performance. It is important to note that classification performance is not the ultimate goal of this study, but rather a target to help structure the latent space. Indeed, we hypothesize that the better the classification scores, the more relevant the underlying representation is for characterizing HT.

1) *XTab Architecture Trained from Scratch Outperforms Other Models*: The design choices that most impact classification performance are the specific architecture configuration and how the weights are initialized. Table I compares two models implementing the FT-Transformer architecture (cf. section IV-C.1). *Tiny FT-Transformer* is optimal while limiting the size of the model, while *XTab* is the configuration used by the foundation model [14]. Table I also includes two weights initialization for each model. In both cases, supervised classification results from randomly initialized weights (*random*) are reported. Pretrained weights depend on the architecture. For the tiny model, weights from self-supervised contrastive pretraining on CARDINAL (cf. fig. 4) are used. For *XTab*, the foundation model's published weights are used.

XTab performs systematically better than the tiny model, with 13 to 38 points more in AUROC depending on the configuration. This shows that the *XTab* architecture is able to generalize well and avoids significantly overfitting, given the similar size between the output features (192D) and the number of training/validation samples (171/20) in our dataset.

As for pretrained weights, specifically the case of *XTab*, they gave surprising results. The model performs better with randomly initialized weights compared to *XTab*'s published weights, improving results between 2.7 and 5.9 points depending on the input data. This suggests that the foundation weights might not generalize well from the domains used for training [14], and that the architecture itself is more important. For the tiny model, pretrained weights were inconclusive, with either positive or negative impact depending on the input data.

Given these results, the following subsections and tables II to IV focus on *XTab* with randomly initialized weights.

2) *Complementary Clinical Data Combined with Time-series Image Descriptors Enables the Best Performance*: To study the role of the data provided to the model, table I reports performance over different configurations of tabular (cf. section IV-C.2) and time-series descriptors (cf. section IV-A). *Tabular descriptors* refer to the subsets of clinical data, while *time-series descriptors* indicate whether unimodal tabular data was used (X) or image-based data was included (✓).

Under the best configuration, i.e. *XTab* with *random weights init.*, the best data configuration is the combination of time-series descriptors with clinical data excluding descriptors derived from echocardiograms (i.e. *w/o echo. data*). This makes sense if we consider that tabular descriptors not derived from images already provide most of the information, evidenced by the unimodal model on *w/o echo. data* reaching 97.4 AUROC. Time-series automatically extracted from echocardiograms are robust and fine-grained enough to provide complementary information to reach 98.0 AUROC. In contrast, tabular descriptors derived from images in *all* add redundancy and noise,

TABLE I: JOINT ABLATION STUDY OF THE DESCRIPTORS PROVIDED AS INPUT, AND OF THE TRANSFORMER ENCODER’S ARCHITECTURE AND WEIGHTS INITIALIZATION. RESULTS CORRESPOND TO THE AUROC’S MEAN \pm STANDARD DEVIATION OVER 10 TRAININGS W/ DIFFERENT SEEDS.

Tabular descriptors	Time-series descriptors	# descriptors	Tiny FT-Transformer [section IV-C.1]			XTab (Large FT-Transformer) [14]		
			random weights init.	pretrained weights init.	# parameters	random weights init.	XTab weights init.	# parameters
all	\times	62	70.8 \pm 7.7	77.9 \pm 3.4	5.2K	96.4 \pm 1.4	91.1 \pm 3.9	898K
	\checkmark	76	58.3 \pm 5.9	71.8 \pm 5.1	6.3K	96.4 \pm 1.3	93.7 \pm 2.6	1 137K
w/o echo. data	\times	28	76.6 \pm 12.1	67.5 \pm 7.9	4.2K	97.4 \pm 1.0	91.5 \pm 3.0	876K
	\checkmark	42	67.0 \pm 6.2	66.8 \pm 10.0	5.4K	98.0 \pm 0.7	93.4 \pm 2.6	1 115K

TABLE II: COMPARISON BETWEEN OUR PIPELINE AND EXISTING METHODS, DEPENDING ON THE INPUT DATA. RESULTS CORRESPOND TO THE AUROC’S MEAN \pm STANDARD DEVIATION OVER 10 TRAININGS W/ DIFFERENT SEEDS, EXCEPT FOR IRENE WHERE THE RESULTS ARE OVER 5 SEEDS, BECAUSE OF COMPUTATIONAL CONSTRAINTS GIVEN THE MODEL’S LARGER SIZE.

Tabular descriptors	Imaging data	Hager <i>et al.</i> [6] (~36.7M param.)	IRENE [17] (~179M param.)	Ours (~1.12M param.)
all	A4C/A2C ED/ES	58.2 \pm 5.2	–	–
	Time-series descriptors	–	87.7 \pm 8.9	96.4 \pm 1.3
w/o echo. data	A4C/A2C ED/ES	59.4 \pm 5.3	–	–
	Time-series descriptors	–	85.1 \pm 4.7	98.0 \pm 0.7

TABLE III: ABLATION STUDY OF CONFIGURATIONS OF TIME-SERIES TOKENIZER AND MULTIMODAL ATTENTION FOR FUSING HETEROGENEOUS DATA. RESULTS CORRESPOND TO THE AUROC’S MEAN \pm STANDARD DEVIATION OVER 10 TRAININGS W/ DIFFERENT SEEDS.

Tabular descriptors	Time-series descriptors	Time-series tokenizer	Bidirectional attention blocks	XTab	
				random weights init.	# parameters
w/o echo. data	\checkmark	linear	\times	92.9 \pm 2.4	891K
			\checkmark	94.7 \pm 2.4	2 079K
		transformer	\times	98.0 \pm 0.7	1 115K
			\checkmark	96.8 \pm 1.8	2 303K

TABLE IV: ABLATION STUDY OF CONFIGURATIONS OF OUTPUT TOKEN REPRESENTATION AND CLASSIFICATION FORMULATION TO STRUCTURE THE POPULATION REPRESENTATION. RESULTS CORRESPOND TO THE AUROC’S MEAN \pm STANDARD DEVIATION OVER 10 TRAININGS W/ DIFFERENT SEEDS.

Tabular descriptors	Time-series descriptors	Token representation	Ordinal constraint	XTab
				random weights init.
w/o echo. data	\checkmark	Sequence pooling	\times	96.5 \pm 2.4
			\checkmark	96.7 \pm 2.7
		[CLS]	\times	97.0 \pm 1.7
			\checkmark	98.0 \pm 0.7

and their number (62 vs 28) complicate the fusion problem, leading to a slight deterioration of the results.

3) *Data Tokenization Leveraging Prior Knowledge Has More Impact Than Multimodal Fusion Strategy*: To study our multimodal pipeline, we start by validating the relevance of working on time-series extracted from image rather than the images directly. Table II compares our model to the state-of-the-art model from Hager *et al.* [6], which combines image and tabular data (cf. section IV-D.1). The results from Hager *et al.* fall drastically below ours, around 38 points in AUROC. This confirms that training multimodal models directly on images for small datasets like ours is inadequate, and that image preprocessing guided by prior knowledge of relevant information, i.e. time-series descriptors, is necessary.

The next component to analyze is then the token fusion strategy. The reference state-of-the-art method in this case is IRENE [17], and its approach to cross-attention with bidirectional attention blocks. Table II also compares our model to IRENE, with its tokenization adapted to use time-series (cf. section IV-D.2). Depending on the tabular subset, our model is better by 9-13 points. We explain IRENE’s worse performance by the fact that, with 179M parameters compared to our model’s 1.1M, it is overparameterized for the task.

Although the full IRENE model underperformed, this alone does not invalidate their bidirectional attention block. Therefore, we tried integrating just this component in our framework (cf. fig. 3), and report the results in table III. Table III also validates another component related to token processing, by testing two configurations of time-series tokenization: a simple *linear* projection and the *time-series transformer* described in section III-A.1. The results show that time-series tokenization has more impact than multimodal attention. The transformer improves results by 2.1-5.1 points, while the impact of bidirectional attention is mixed. Notably, bidirectional attention improves results for the linear tokenizer, but degrades the transformer’s performance. This means that bidirectional attention can extract better information from time-series descriptors when linear tokenization is used. In contrast, results are good enough with the transformer tokenizer that bidirectional attention does not improve them. Rather, the parameters increase, more than doubling the model’s size, becomes too much and

leads to worse results.

4) *Best Representation Is Obtained by [CLS] Token with Ordinal Constraint*: The final component left to discuss is how output features are represented and constrained. Regarding the definition of output features, table IV compares the standard [CLS] token with sequence pooling [29], which computes a dynamic average of all output tokens, similar to the fixed averaging done by IRENE [17]. The impact of the ordinal constraint on both output representations is also reported.

The [CLS] token provides slightly better and more stable results over sequence pooling, with 0.5-1.3 increases in mean AUROC and 0.7-2.0 decreases in standard deviation. Regarding the ordinal constraint, Beckham and Pal explained that their formulation regularizes the predicted probabilities, which might not help top-1 accuracy but would improve scores that rely on the probabilities over multiple labels, such as top- k accuracy or AUROC [27]. Our results support their rationale, with the ordinal constraint increasing AUROC by 0.2-1.0 points over a standard classification head.

These improvements might appear small given the large impacts of the architecture and input data. However, considering the high absolute scores, ranging between 96.5 and 98.0, these differences are substantial.

B. Continuous Stratification Interpretability

As mentioned earlier, we optimized our framework’s classification scores, assuming that the model with the highest classification accuracy would also most effectively characterize hypertension. The ablation studies discussed in section V-A allowed us to identify an optimal configuration (in bold in tables I to IV). Since we trained each configuration 10 times, we had to select the most representative model out of the 10. We defined it as the model with the smallest MAE between its predicted p for each patient and the average p across the 10 models. In the next subsections, we study the properties of this model’s latent representation to see if it can reveal new, clinically interpretable markers of hypertension.

1) Stratification Fuzziness Correlates to Model Variability:

When computing the MAE described above on the models’ predicted stratifications p , the predictions vary on average by only 3.6%. Given that, to the best of our knowledge, no previous work on classifying/phenotyping cardiovascular populations studied the robustness of their representation across trainings [8], [25], [35], we consider this result significant.

To understand how the variability between models manifests itself on a per patient basis, we look at the standard deviation (SD) between models’ predicted stratifications. Figure 7 plots this SD on each patient w.r.t. the stratification predicted by the representative model. This highlights that the variability is not constant along the stratification domain, e.g. a uniform band. The variability is higher near the transition zones, i.e. around 0.35 and 0.7 on the x-axis, and gradually decreases on both sides of these transitions, the more the model is confident about its prediction. Still, this increase in SD is much more striking in the transition from *controlled* and *uncontrolled* patients than from *wht* to *controlled* patients. We attribute this to the models not being as confident overall in their predictions

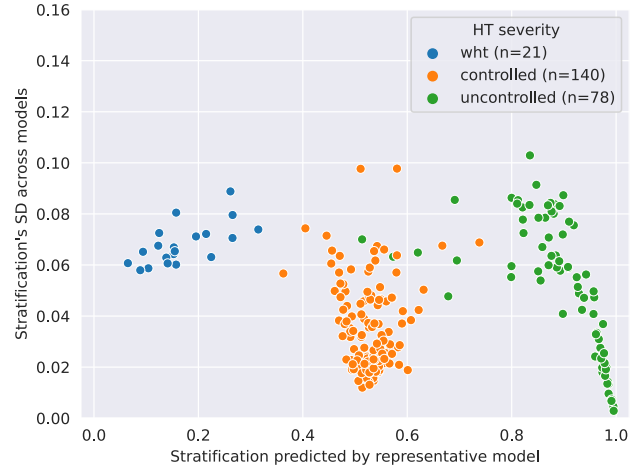


Fig. 7: Visualization of the continuous stratification prediction’s standard deviation (SD) across multiple trainings of the same model w.r.t. the predictions of the most representative model. The standard deviation tends to increase for patients near the frontier between 2 labels, especially between controlled and uncontrolled, meaning that patients considered ambiguous by the best model are indeed stratified with more variability across the ensemble of models.

for *wht* patients. Indeed, the SD for *wht* patients is between 0.06-0.09, whereas it can go as low as 0-0.01 for *controlled* or *uncontrolled* patients. This is probably due to the fact that there are relatively few *wht* patients ($n=21$).

This result is desirable, because it shows that when the stratification by the representative model suggests fuzzy associations to target labels, it correlates with a higher variability in stratification across the set of models. This indicates that the representative model’s confidence is representative of the framework’s variability. It is further proof that the representation learned by our model achieved the stated goal of stratifying the patients beyond the provided target labels.

2) *Continuum Highlights New Prospective Markers of Hypertension in Time-series*: Figure 8 studies patterns on two time-series descriptors with respect to both the target labels and continuous stratification, Global Longitudinal Strain (GLS) and Basal Septal Thickness (BST), which are important parameters of left ventricular function and remodeling [4], [34].

GLS measures the deformation of the myocardium as the [negative] ratio of the contraction along its contour w.r.t. when the ventricle is most dilated at ED. Cardiologists often use the smallest GLS value, the peak GLS, as a biomarker of systolic function, along with ejection fraction (EF), i.e. the ratio of the variation of the volume of the ventricle. However, using the full GLS curve, instead of the scalar peak GLS and EF, can provide a more detailed analysis of the specific mechanisms affected by HT [36]. BST presents a similar story. It measures the thickness of the myocardium at the base of the septum, i.e. the wall between the left and right ventricles. The septum can become thicker in patients suffering from HT, as a response to the increased pressure (afterload) from the LV side [34]. BST is measured statically in typical clinical workflows (from parasternal acquisitions), but studying its variation over the cardiac cycle could provide additional insights.

Figures 8a and 8b present average GLS curves over target

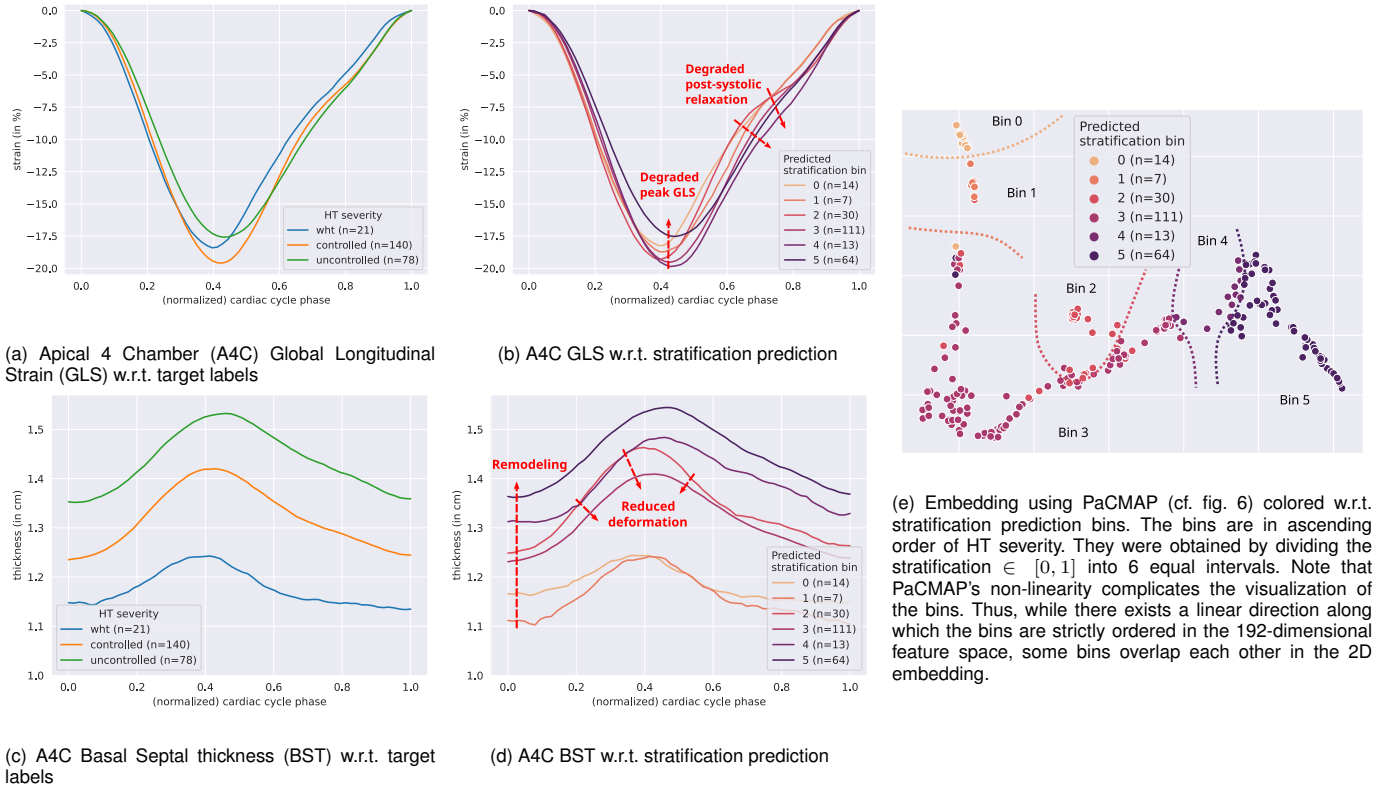


Fig. 8: Illustration of the repercussions of HT severity on cardiac function descriptors. Each plot shows the average curve for one cardiac function descriptor by groups of patients (whose sizes are specified in the legends). The patient groups are determined either based on the reference HT severity labels [(a) and (c)], or on discrete bins of our continuous stratification [(b) and (d)]. (e) represents the same embedding as in fig. 6, but w.r.t. the stratification bins. Both sets of figures display ranges of phenotypes, but the continuous stratification describes in more incremental steps the evolution from normotensive cases (*wht*/0) to severe HT (*uncontrolled*/5).

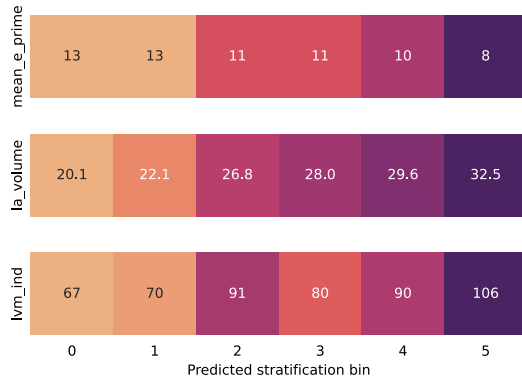


Fig. 9: Heatmaps of scalar cardiac function descriptors known to be linked to HT (left), averaged over bins extracted from our continuous stratification (bottom, cf. fig. 8e). Colors show the progression from normal values (light) to pathological values (dark).

HT severity labels and a discretized version of the continuous stratification from our method (cf. fig. 8e). Two markers related to HT severity can be observed in these curves. The first one is that peak GLS actually improves in controlled patients compared to normotensive subjects (*wht*), likely due to their hypertensive treatment. Peak GLS then degrades for uncontrolled patients, once their treatment no longer manages the effects of HT. This first marker is observable using both the target labels (fig. 8a) and the continuous stratification

(fig. 8b). However, only the continuous stratification highlights the second marker, namely the degradation of post-systolic relaxation in intermediate to early severe cases (bins 2-4). Post-systolic relaxation is measured through the slope of the strain curve after systole, i.e. between 0.4 and 0.7 on the x-axis, with healthier subjects presenting earlier, sharper slopes. Thus, while bins 2-4 present similar peak GLS, post-systolic relaxation gradually happens later and slower. Thus, thanks to our continuous stratification approach, we highlighted that post-systolic relaxation could be an early marker of worsening HT, before meaningful changes in peak GLS.

Figures 8c and 8d show similar curves, but for septal thickness. Again, both the target labels and continuous stratification exhibit similar tendencies, with BST being overall correlated to HT severity. However, the granularity on intermediate to early severe cases (bins 2-4) suggests the relation between BST and HT severity might not be linear. The septum of patients in bin 2 thickens more during end-systole, around 0.4 on the x-axis, than that of patients in bin 3. In other terms, on the CARDINAL cohort, HT first leads to a less deformable septum, before the septum thickens to accommodate the higher pressure. These results confirm the established notion that HT leads to septal remodeling [34], while suggesting that altered deformation patterns could also be markers of HT progression.

3) *Continuum Reranks Importance of Tabular Markers of Hypertension*: Finally, fig. 9 presents an analogous study on scalar cardiac function descriptors. An expert cardiologist an-

alyzed the tabular descriptors, aggregated with respect to bins on our continuous stratification (cf. fig. 8e), to see if relevant tendencies existed across the bins. Three parameters linked to HT [2] were of particular interest: average mitral annulus velocity (*mean_e_prime*), left atrium volume (*la_volume*), and indexed LV mass (*lvm_ind*). While *lvm_ind* is usually the measure most relied upon, fig. 9 illustrates that it does not always progress linearly with HT severity, unlike the two other descriptors. This locally non-linear relationship could not be identified from the target HT severity labels because they group too many patients together. Therefore, our continuous stratification paves the way for renewed investigations into the predictive power of known scalar markers.

VI. DISCUSSION AND CONCLUSION

In this work, we proposed a framework for fusing multimodal tabular and 2D+time echocardiograms to learn a continuous stratification of patients, given limited data with categorical labels. The framework is designed to target difficult-to-characterize pathologies by, on one hand, combining complementary descriptors derived from images and EHRs, and, on the other hand, projecting the patients along an interpretable pathological continuum.

We built our approach to multimodal fusion around tabular transformers. Inspired by mid-fusion methods, imaging data is first processed into additional scalar and time-series descriptors, that are then tokenized and combined to tabular tokens. We showed that, in the context of our application, this kind of tokenization with strong inductive bias based on prior knowledge of the application appears to be preferable to generic multimodal fusion strategies. For our model's backbone, we relied on the architecture of the XTab foundation model for tabular data. Surprisingly, it performed better, in our limited data setting, than smaller models with a similar architecture. It even performed best when trained from scratch, rather than using the foundation model's pretrained weights. These findings hint at a generalizability of the XTab architecture, even on small datasets, that warrants further research. We also formulated an ordinal classification objective to integrate the order of the labels in the structure of the latent representation. This additional guidance from the labels marginally improved performance, on top of providing the desired continuously interpretable stratification. Finally, we showed that the phenotypes extracted from the continuous stratification are coherent with prior physiological knowledge, i.e. phenotypes of the target labels, while allowing for more detailed analysis of the local variations within established phenotypes.

Compared to previous works, our approach stands out by working with tabular and imaging data, and by predicting a precise stratification of patients. The work most directly comparable to ours is the IRENE multimodal transformer [17], which fuses images and unstructured medical records to classify pulmonary diseases. However, their dataset of over 44K samples allowed them to train a large model directly on images and unstructured medical records. In our case, the poor performance of Hager *et al.*'s model [6], a state-of-the-art method for combining imaging and tabular data, demonstrates

that our dataset is too limited to work directly on images. Therefore, we implemented a pipeline leveraging prior expert knowledge to extract relevant descriptors from images and EHRs. On top of that, we also used a much smaller transformer architecture to significantly outperform IRENE when trained on the same pre-processed data.

A. Limitations

Compared to competing state-of-the-art methods [6], [7], [17], which are trained on at least thousands of samples, one possible criticism against our study is the limited size of the CARDINAL dataset. We would argue that CARDINAL is typical of pilot clinical studies in cardiac imaging. First, its size is in line with the scale of other targeted clinical cohorts [25]. Second, despite its size, CARDINAL aims to provide representative samples from all over the HT continuum. By contrast, the large datasets used by comparable methods are aimed at multi-disease classification, with no notion of disease progression. Given our stated goals, the use of the CARDINAL dataset is justified over other, potentially much larger, datasets. Because of this, a pipeline like ours, which can outperform more generic, larger-scale state-of-the-art methods and achieve excellent results on datasets like CARDINAL, is highly relevant for pilot clinical studies.

B. Conclusion

We presented a framework that learns a stratification of hypertensive patients by fusing 2D+time echocardiographic images with structured medical records data. We tailored our method to difficult-to-characterize pathologies by using ordinal classification to learn a continuous stratification. We showed that our continuous stratification provides better insights into how hypertension impacts clinically-relevant cardiac shape and motion descriptors than reference labels, which might miss or mischaracterize alterations of these descriptors. In the end, we hope these insights inspire further works into characterizing full pathological continuums, rather than discrete stages, from all the multimodal data available in healthcare settings.

ACKNOWLEDGMENT

The authors thank Elisa Le Maout (ARC, Hôpital Lyon Sud, Hospices Civils de Lyon, Lyon, France) for her help with data collection for the CARDINAL dataset.

REFERENCES

- [1] C. Pellegrini, N. Navab, and A. Kazi, "Unsupervised pre-training of graph transformers on patient population graphs," *Med Image Anal*, vol. 89, p. 102895, Oct. 2023.
- [2] G. Mancina *et al.*, "2023 ESH Guidelines for the management of arterial hypertension The Task Force for the management of arterial hypertension of the European Society of Hypertension," *J. Hypertens.*, vol. 41, p. 1874, Dec. 2023.
- [3] M. Sermesant, H. Delingette, H. Cochet, P. Jaïs, and N. Ayache, "Applications of artificial intelligence in cardiovascular imaging," *Nat Rev Cardiol*, vol. 18, pp. 600–9, Aug. 2021.
- [4] I. M. Salte *et al.*, "Artificial Intelligence for Automatic Measurement of Left Ventricular Strain in Echocardiography," *JACC Cardiovasc Imaging*, vol. 14, pp. 1918–28, Oct. 2021.

- [5] H. J. Ling, N. Painchaud, P.-Y. Courand, P.-M. Jodoin, D. Garcia, and O. Bernard, "Extraction of Volumetric Indices from Echocardiography: Which Deep Learning Solution for Clinical Use?" in *Proc. FIMH*, 2023, pp. 245–54.
- [6] P. Hager, M. J. Menten, and D. Rueckert, "Best of Both Worlds: Multimodal Contrastive Learning With Tabular and Imaging Data," in *Proc. CVPR*, 2023, pp. 23 924–35.
- [7] J. Schilcher, A. Nilsson, O. Andlid, and A. Eklund, "Fusion of electronic health records and radiographic images for a multimodal deep learning prediction model of atypical femur fractures," *Comput Biol Med*, vol. 168, p. 107704, Jan. 2024.
- [8] Q. Zheng, H. Delingette, K. Fung, S. E. Petersen, and N. Ayache, "Pathological Cluster Identification by Unsupervised Analysis in 3,822 UK Biobank Cardiac MRIs," *Front Cardiovasc Med*, vol. 7, 2020.
- [9] A. Kline *et al.*, "Multimodal machine learning in precision health: A scoping review," *npj Digit. Med.*, vol. 5, pp. 1–14, Nov. 2022.
- [10] P. Rajpurkar, E. Chen, O. Banerjee, and E. J. Topol, "AI in health and medicine," *Nat Med*, vol. 28, pp. 31–8, Jan. 2022.
- [11] P. Xu, X. Zhu, and D. A. Clifton, "Multimodal Learning With Transformers: A Survey," *IEEE PAMI*, vol. 45, pp. 12 113–32, Oct. 2023.
- [12] Q. Wen *et al.*, "Transformers in Time Series: A Survey," in *Proc. IJCAI*, vol. 6, 2023, pp. 6778–86.
- [13] Y. Gorishniy, I. Rubachev, V. Khrulkov, and A. Babenko, "Revisiting Deep Learning Models for Tabular Data," in *Proc. NeurIPS*, vol. 34, 2021.
- [14] B. Zhu, X. Shi, N. Erickson, M. Li, G. Karypis, and M. Shoaran, "XTab: Cross-table Pretraining for Tabular Transformers," in *Proc. ICML*, 2023, pp. 43 181–204.
- [15] S. Zhang and D. Metaxas, "On the challenges and perspectives of foundation models for medical image analysis," *Med Image Anal*, vol. 91, p. 102996, Jan. 2024.
- [16] T. Baltrušaitis, C. Ahuja, and L.-P. Morency, "Multimodal Machine Learning: A Survey and Taxonomy," *IEEE PAMI*, vol. 41, pp. 423–43, Feb. 2019.
- [17] H.-Y. Zhou *et al.*, "A transformer-based representation-learning model with unified processing of multimodal input for clinical diagnostics," *Nat. Biomed. Eng.*, vol. 7, pp. 743–55, Jun. 2023.
- [18] D. Bahri, H. Jiang, Y. Tay, and D. Metzler, "Scarf: Self-Supervised Contrastive Learning using Random Feature Corruption," in *Proc. ICLR*, 2022.
- [19] A. Nagrani, S. Yang, A. Arnab, A. Jansen, C. Schmid, and C. Sun, "Attention Bottlenecks for Multimodal Fusion," in *Proc. NeurIPS*, vol. 34, 2021, pp. 14 200–13.
- [20] S.-C. Huang, A. Pareek, S. Seyyedi, I. Banerjee, and M. P. Lungren, "Fusion of medical imaging and electronic health records using deep learning: a systematic review and implementation guidelines," *npj Digit. Med.*, vol. 3, pp. 1–9, Oct. 2020.
- [21] D. E. Schlesinger and C. M. Stultz, "Deep Learning for Cardiovascular Risk Stratification," *Curr Treat Options Cardio Med*, vol. 22, p. 15, Jun. 2020.
- [22] I. Landi *et al.*, "Deep representation learning of electronic health records to unlock patient stratification at scale," *npj Digit. Med.*, vol. 3, pp. 1–11, Jul. 2020.
- [23] L. Oakden-Rayner, J. Dunnmon, G. Carneiro, and C. Re, "Hidden stratification causes clinically meaningful failures in machine learning for medical imaging," in *Proc. ACM Int. Conf. Inf. Knowl. Manag.*, 2020, pp. 151–9.
- [24] S. Sanchez-Martinez *et al.*, "Machine Learning for Clinical Decision-Making: Challenges and Opportunities in Cardiovascular Imaging," *Front Cardiovasc Med*, vol. 8, 2022.
- [25] F. Loncaric *et al.*, "Automated Pattern Recognition in Whole-Cardiac Cycle Echocardiographic Data: Capturing Functional Phenotypes with Machine Learning," *JASE*, vol. 34, pp. 1170–83, Nov. 2021.
- [26] T. Tran, D. Phung, W. Luo, and S. Venkatesh, "Stabilized sparse ordinal regression for medical risk stratification," *Knowl Inf Syst*, vol. 43, pp. 555–82, Jun. 2015.
- [27] C. Beckham and C. Pal, "Unimodal Probability Distributions for Deep Ordinal Classification," in *Proc. ICML*, 2017, pp. 411–9.
- [28] Y. Wang, H. Huang, C. Rudin, and Y. Shaposhnik, "Understanding How Dimension Reduction Tools Work: An Empirical Approach to Deciphering t-SNE, UMAP, TriMap, and PaCMAP for Data Visualization," *JMLR*, vol. 22, pp. 1–73, 2021.
- [29] A. Hassani, S. Walton, N. Shah, A. Abuduweili, J. Li, and H. Shi, "Escaping the Big Data Paradigm with Compact Transformers," Jun. 2022, arXiv:2104.05704 [cs.CV].
- [30] P. Gijsbers *et al.*, "AMLB: an AutoML Benchmark," Nov. 2023, arXiv:2207.12560 [cs.LG].
- [31] S. Onishi and S. Meguro, "Rethinking Data Augmentation for Tabular Data in Deep Learning," May 2023, arXiv:2305.10308 [cs.LG].
- [32] T. Chen, S. Kornblith, M. Norouzi, and G. Hinton, "A Simple Framework for Contrastive Learning of Visual Representations," in *Proc. ICML*, vol. 119, 2020, pp. 1597–607.
- [33] E. D. Folland, A. F. Parisi, P. F. Moynihan, D. R. Jones, C. L. Feldman, and D. E. Tow, "Assessment of left ventricular ejection fraction and volumes by real-time, two-dimensional echocardiography. A comparison of cineangiographic and radionuclide techniques," *Circulation*, vol. 60, pp. 760–6, Oct. 1979.
- [34] M. Marciniak *et al.*, "Septal curvature as a robust and reproducible marker for basal septal hypertrophy," *J. Hypertens.*, vol. 39, p. 1421, Jul. 2021.
- [35] S. J. Shah *et al.*, "Phenomapping for Novel Classification of Heart Failure With Preserved Ejection Fraction," *Circulation*, vol. 131, pp. 269–79, Jan. 2015.
- [36] M. Cikes, G. R. Sutherland, L. J. Anderson, and B. H. Bijns, "The role of echocardiographic deformation imaging in hypertrophic myopathies," *Nat Rev Cardiol*, vol. 7, pp. 384–96, Jul. 2010.

TABLE V: LIST OF THE 46 PATIENT DESCRIPTORS FOR THE CARDINAL DATASET EXTRACTED FROM ELECTRONIC HEALTH RECORDS (EHRs). THE DESCRIPTORS ARE CATEGORIZED BY THE EXAMS/RECORDS FROM WHICH THEY ARE OBTAINED. IN THIS CASE, THE DESCRIPTORS COMING FROM IMAGES, I.E. TTE, WERE MANUALLY MEASURED AS PART OF THE CLINICAL WORKFLOW.

Source	Abbreviation (in code/figures)	Unit/labels	Description
General info	age	years	Age
	sex	M/W	Sex
	bmi	kg/m ²	Body Mass Index (BMI)
Medical history	hf	yes/no	Heart Failure
	cad	yes/no	Coronary Artery Disease (CAD)
	pad	yes/no	Peripheral Artery Disease (PAD)
	stroke	yes/no	Stroke
	tobacco	none/ceased/active	Tobacco
	diabetes	yes/no	Diabetes
	dyslipidemia	yes/no	Dyslipidemia
Holter monitor	sbp_24	mmHg	Systolic Blood Pressure (SBP) averaged over 24h
	dbp_24	mmHg	Diastolic Blood Pressure (DBP) averaged over 24h
	pp_24	mmHg	Pulse Pressure (PP) averaged over 24h
Biological exam	creat	μmol/L	Plasma CREATinine level
	gfr	mL/min/1.73m ²	Glomerular Filtration Rate (GFR) indexed to standard body surface area (1.73m ²)
	nt_probnp	pg/mL	Molar ratio of NT-proBNP
Treatment	ddd	–	Defined Daily Dose (DDD) of blood pressure medication
	bradycardic	yes/no	Medication includes bradycardic agents (beta-blockers, diltiazem or verapamil)
	ace_inhibitor	yes/no	Medication includes Angiotensin-Converting Enzyme (ACE) inhibitors
	arb	yes/no	Medication includes Angiotensin Receptor Blockers (ARB)
	tz_diuretic	yes/no	Medication includes Thiazide (TZ) diuretics
	central_acting	yes/no	Medication includes central-acting agents
	beta_blocker	yes/no	Medication includes beta blockers
	spironolactone	yes/no	Medication includes spironolactone
	alpha_blocker	yes/no	Medication includes alpha blockers
Trans thoracic echocardiogram (TTE)	ccb	yes/no	Medication includes Calcium Channel Blockers (CCB)
	sbp_tte	mmHg	Systolic Blood Pressure (SBP) during TTE
	dpb_tte	mmHg	Diastolic Blood Pressure (SBP) during TTE
	pp_tte	mmHg	Pulse Pressure (SBP) during TTE
	hr_tte	Beats Per Minute (BPM)	Heart Rate (HR) during TTE
	e_velocity	m/s	E-wave (passive blood flow from left atrium to left ventricle) velocity
	a_velocity	m/s	A-wave (active blood flow caused by atrial contraction) velocity
	mv_dt	millisecond	Mitral Valve (MV) Deceleration Time (DT)
	lateral_e_prime	cm/s	Lateral mitral annular velocity (e')
	septal_e_prime	cm/s	Septal mitral annular velocity (e')
	reduced_e_prime	yes/no	Reduced E': lateral e' < 10 cm/s or septal e' < 7 cm/s
	e_e_prime_ratio	–	Ratio of E velocity over e': E/e'
	d_dysfunction_e_e_prime_ratio	yes/no	High ratio of E/e' indicating Diastolic dysfunction: E/e' > 14
	la_volume	mL/m ²	Left Atrial (LA) volume indexed to body surface area (BSA)
	dilated_la	yes/no	Dilated LA volume indexed to BSA indicating diastolic dysfunction: $la_volume > 34 \text{ mL/m}^2$
	ph_vmax_tr	yes/no	Pulmonary Hypertension (PH) indicated by peak Tricuspid Regurgitation (TR): $TR > 2.8 \text{ m/s}$
	lv_m_ind	g/m ²	Left Ventricular Mass (LVM) indexed to BSA
	lvh	yes/no	Left Ventricular Hypertrophy (LVH)
	ivs_d	cm	InterVentricular Septum (IVS) thickness at end-Diastole (D)
	lvid_d	cm	Left Ventricular Internal Diameter (LVID) at end-Diastole (D)
	pw_d	cm	Left ventricular Posterior Wall (PW) thickness at end-Diastole (D)

TABLE VI: LIST OF THE 7 PATIENT DESCRIPTORS FOR THE CARDINAL DATASET DERIVED FROM A POSTERIOR ASSESSMENT BY A CARDIOLOGIST.

Source	Abbreviation (in code/figures)	Labels	Description
Hypertension assessment	etiology	essential secondary pa	Etiology of the HyperTension (HT): <i>essential</i> : HT without one distinct cause <i>secondary</i> : HT related to endocrine, renal or renovascular conditions <i>pa</i> : HT caused by Primary hyperAldosteronism (PA)
	nt_probnp_group	neutral end_organ_damage mortality_rate	Correlation with potential outcomes based on NT-proBNP rate: <i>neutral</i> : No known adverse effects <i>end_organ_damage</i> : Risk of at least one end/target organ impacted by HT (> 90 pg/mL for men, > 142 pg/mL for women) <i>mortality_rate</i> : Risk of mortality (> 150 pg/mL)
	ht_grade	0–3	Classification of HT based on measured Blood Pressure (BP) over 24h: <i>0 (normal)</i> : Systolic BP < 130 mmHg and/or Diastolic BP < 80 mmHg <i>Grade 1 HT</i> : 130-149 SBP and/or 80-89 DBP <i>Grade 2 HT</i> : 150-169 SBP and/or 90-99 DBP <i>Grade 3 HT</i> : SBP \geq 170 and/or DBP \geq 100
	ht_severity	wht controlled uncontrolled	Severity of HT manually determined by a cardiologist: <i>wht</i> : no positive diagnosis of HT (White coat HyperTension) <i>controlled</i> : under the recommended blood pressure level given the treatment (grade 1 or lower) <i>uncontrolled</i> : above the recommended blood pressure level despite the treatment (grade 2 or higher)
	diastolic_dysfunction_param_sum	0–4	1 point per parameter of diastolic dysfunction (cf. table V): <i>dilated_la</i> , <i>reduced_e_prime</i> , <i>d_dysfunction_e_e_prime_ratio</i> , <i>ph_vmax_tr</i>
	diastolic_dysfunction	none uncertain certain	Diagnosis of diastolic dysfunction, based on the sum of parameters: <i>none</i> : 0 or 1 parameter <i>uncertain</i> : 2 parameters <i>certain</i> : 3 or 4 parameters
	ht_cm	none uncertain certain	Diagnosis of HyperTensive CardioMyopathy (HT-CM) based on TTE analysis: <i>none</i> : no diastolic dysfunction and no Left Ventricular Hypertrophy (LVH) <i>uncertain</i> : uncertain diastolic dysfunction and no LVH <i>certain</i> : certain diastolic dysfunction and/or LVH

TABLE VII: LIST OF THE 25 PATIENT DESCRIPTORS EXTRACTED FROM SEGMENTATIONS OF TRANSTHORACIC ECHOCARDIOGRAM (TTE) FOR THE CARDINAL DATASET. THE DESCRIPTORS ARE CATEGORIZED BY WHETHER THEY ARE GLOBAL BIOMARKERS (*Scalar*), OR EXTRACTED FRAME-BY-FRAME (*Time-series*). IN THIS CASE, ALL DESCRIPTORS WERE EXTRACTED AUTOMATICALLY FROM LEFT VENTRICLE AND MYOCARDIUM SEGMENTATIONS.

Type	Abbreviation (in code/figures)	Unit	Count	Input views			Description
				A4C	A2C	A4C+A2C	
Scalar	edv	mL	1			✓	End-Diastole (ED) Volume (V) of the Left Ventricle (LV)
	esv	mL	1			✓	End-Systole (ES) Volume of the LV
	ef	%	1			✓	Ejection Fraction (EF) of the LV
	a4c_ed_sc_[min max] a4c_ed_lc_[min max]	dm ⁻¹	4	✓			Min./max. myocardial curvature at the base of each wall in A4C ED: <i>A4C left wall</i> : septum (s) / <i>A4C right wall</i> : lateral (l)
	a2c_ed_ic_[min max] a2c_ed_ac_[min max]	dm ⁻¹	4		✓		Min./max. myocardial curvature at the base of each wall in A2C ED: <i>A2C left wall</i> : inferior (i) / <i>A2C right wall</i> : anterior (a)
Time-series	lv_area	cm ²	2	✓	✓		Surface area of the LV
	lv_length	cm	2	✓	✓		Distance between the LV's apex and midpoint at the base
	gls	%	2	✓	✓		Global Longitudinal Strain (GLS)
	ls_left	%	2	✓	✓		Regional Longitudinal Strain (LS) at the base of the left wall <i>A4C left wall</i> : septum / <i>A2C left wall</i> : inferior
	ls_right	%	2	✓	✓		Regional Longitudinal Strain (LS) at the base of the right wall <i>A4C right wall</i> : lateral / <i>A2C right wall</i> : anterior
	myo_thickness_left	cm	2	✓	✓		Average myocardial thickness at the base of the left wall <i>A4C left wall</i> : septum / <i>A2C left wall</i> : inferior
	myo_thickness_right	cm	2	✓	✓		Average myocardial thickness at the base of the right wall <i>A4C right wall</i> : lateral / <i>A2C right wall</i> : anterior